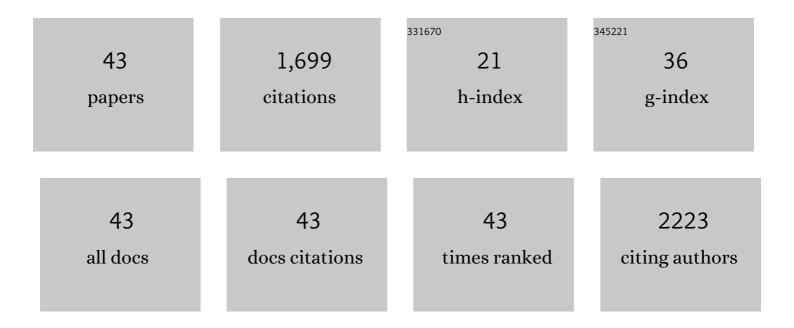
## Weizong Xu

List of Publications by Year in descending order

Source: https://exaly.com/author-pdf/7195936/publications.pdf Version: 2024-02-01



WEIZONC XII

#	Article	IF	CITATIONS
1	Ultrastrong Mg Alloy via Nano-spaced Stacking Faults. Materials Research Letters, 2013, 1, 61-66.	8.7	268
2	Effect of carbon nanotube length on thermal, electrical and mechanical properties of CNT/bismaleimide composites. Carbon, 2013, 53, 145-152.	10.3	166
3	Significant hardening due to the formation of a sigma phase matrix in a high entropy alloy. Intermetallics, 2013, 33, 81-86.	3.9	153
4	In-situ atomic-scale observation of irradiation-induced void formation. Nature Communications, 2013, 4, 2288.	12.8	98
5	Effect of Ag on interfacial segregation in Mg–Gd–Y–(Ag)–Zr alloy. Acta Materialia, 2015, 95, 20-29.	7.9	95
6	Morphology, structure and composition of precipitates in Al0.3CoCrCu0.5FeNi high-entropy alloy. Intermetallics, 2013, 32, 329-336.	3.9	82
7	Physics and model of strengthening by parallel stacking faults. Applied Physics Letters, 2013, 103, .	3.3	81
8	Grain Size Effect on Deformation Mechanisms of Nanocrystalline bcc Metals. Materials Research Letters, 2013, 1, 26-31.	8.7	78
9	Carbide characterization in a Nb-microalloyed advanced ultrahigh strength steel after quenching–partitioning–tempering process. Materials Science & Engineering A: Structural Materials: Properties, Microstructure and Processing, 2010, 527, 3373-3378.	5.6	58
10	Strong and Conductive Dry Carbon Nanotube Films by Microcombing. Small, 2015, 11, 3830-3836.	10.0	56
11	Quantitative atomic resolution elemental mapping via absolute-scale energy dispersive X-ray spectroscopy. Ultramicroscopy, 2016, 168, 7-16.	1.9	49
12	A deep convolutional neural network to analyze position averaged convergent beam electron diffraction patterns. Ultramicroscopy, 2018, 188, 59-69.	1.9	47
13	Measurement of microstructural parameters of nanocrystalline Fe–30wt.%Ni alloy produced by surface mechanical attrition treatment. Journal of Alloys and Compounds, 2009, 474, 546-550.	5.5	45
14	Calcination Temperature Dependent Catalytic Activity and Stability of IrO <sub>2</sub> –Ta <sub>2</sub> O <sub>5</sub> Anodes for Oxygen Evolution Reaction in Aqueous Sulfate Electrolytes. Journal of the Electrochemical Society, 2017, 164, F895-F900.	2.9	42
15	High-temperature grain size stabilization of nanocrystalline Fe–Cr alloys with Hf additions. Materials Science & Engineering A: Structural Materials: Properties, Microstructure and Processing, 2014, 613, 289-295.	5.6	36
16	Size effect of primary Y2O3 additions on the characteristics of the nanostructured ferritic ODS alloys: Comparing as-milled and as-milled/annealed alloys using S/TEM. Journal of Nuclear Materials, 2014, 452, 223-229.	2.7	34
17	Structure and chemistry of passivated SiC/SiO2 interfaces. Applied Physics Letters, 2016, 108, 201607.	3.3	34
18	Direct conversion of h-BN into c-BN and formation of epitaxial c-BN/diamond heterostructures. Journal of Applied Physics, 2016, 119, .	2.5	31

WEIZONG XU

#	Article	IF	CITATIONS
19	Deformation-induced ω phase in nanocrystalline Mo. Scripta Materialia, 2013, 68, 130-133.	5.2	29
20	Dislocations with edge components in nanocrystalline bcc Mo. Journal of Materials Research, 2013, 28, 1820-1826.	2.6	28
21	Influence of scandium addition on the high-temperature grain size stabilization of oxide-dispersion-strengthened (ODS) ferritic alloy. Materials Science & Engineering A: Structural Materials: Properties, Microstructure and Processing, 2015, 636, 565-571.	5.6	23
22	Nucleation and growth mechanism of Ag precipitates in a CuAgZr alloy. Materials Science & Engineering A: Structural Materials: Properties, Microstructure and Processing, 2014, 610, 85-90.	5.6	22
23	Effect of nano-oxide particle size on radiation resistance of iron–chromium alloys. Journal of Nuclear Materials, 2016, 469, 72-81.	2.7	21
24	Microstructures and Stabilization Mechanisms of Nanocrystalline Iron-Chromium Alloys with Hafnium Addition. Metallurgical and Materials Transactions A: Physical Metallurgy and Materials Science, 2015, 46, 4394-4404.	2.2	20
25	A numerical model for multiple detector energy dispersive X-ray spectroscopy in the transmission electron microscope. Ultramicroscopy, 2016, 164, 51-61.	1.9	19
26	In-situ real-space imaging of single crystal surface reconstructions via electron microscopy. Applied Physics Letters, 2016, 109, 201601.	3.3	17
27	On the origin and behavior of irradiation-induced c-component dislocation loops in magnesium. Acta Materialia, 2017, 131, 457-466.	7.9	16
28	Finite element simulation and experimental investigation on homogeneity of Mg-9.8Gd-2.7Y-0.4Zr magnesium alloy processed by repeated-upsetting. Journal of Materials Processing Technology, 2015, 225, 310-317.	6.3	12
29	Influence of experimental conditions on atom column visibility in energy dispersive X-ray spectroscopy. Ultramicroscopy, 2016, 171, 1-7.	1.9	10
30	Dynamic Void Growth and Shrinkage in Mg under Electron Irradiation. Materials Research Letters, 2014, 2, 176-183.	8.7	7
31	Long-term stability of 14YT–4Sc alloy at high temperature. Materials Science & Engineering A: Structural Materials: Properties, Microstructure and Processing, 2015, 647, 222-228.	5.6	7
32	Numerical modeling of specimen geometry for quantitative energy dispersive X-ray spectroscopy. Ultramicroscopy, 2018, 184, 100-108.	1.9	6
33	Twinning in cryomilled nanocrystalline Mg powder. Philosophical Magazine Letters, 2013, 93, 457-464.	1.2	5
34	A Convolutional Neural Network Approach to Thickness Determination using Position Averaged Convergent Beam Electron Diffraction. Microscopy and Microanalysis, 2017, 23, 120-121.	0.4	2
35	In-situ-by-Ex-situ: FIB-less Preparation of Bulk Samples on Heating Membranes for Atomic Resolution STEM Imaging. Microscopy and Microanalysis, 2016, 22, 774-775.	0.4	1
36	Absolute-Scale Comparison with Simulation for Quantitative Energy-Dispersive X-Ray Spectroscopy in Atomic-Resolution Scanning Transmission Electron Microscopy. Microscopy and Microanalysis, 2017, 23, 388-389.	0.4	1

WEIZONG XU

#	Article	IF	CITATIONS
37	Influence of Convergence Angle and Finite Effective Source Size for Quantitative Atomic Resolution EDXS. Microscopy and Microanalysis, 2015, 21, 1093-1094.	0.4	0
38	Effect of Specimen Geometry on Quantitative EDS Analysis with Four-Quadrant Super-X Detectors. Microscopy and Microanalysis, 2015, 21, 1091-1092.	0.4	0
39	Resolving Atomic Scale Chemistry and Structure at NO and Ba Passivated SiC/SiO 2 Interfaces. Microscopy and Microanalysis, 2016, 22, 1658-1659.	0.4	Ο
40	Standardless EDS Composition Analysis using Quantitative Annular Dark-Field Imaging. Microscopy and Microanalysis, 2017, 23, 512-513.	0.4	0
41	Novel FIB-less Fabrication of Electrical Devices for in-situ Biasing. Microscopy and Microanalysis, 2017, 23, 1502-1503.	0.4	Ο
42	Numerical Modeling of Specimen Geometry for Quantitative Multiple Detector EDS. Microscopy and Microanalysis, 2017, 23, 390-391.	0.4	0
43	Utilizing High-temperature Atomic-resolution STEM and EELS to Determine Reconstructed Surface Structure of Complex Oxide. Microscopy and Microanalysis, 2017, 23, 1596-1597.	0.4	0